

The Tunable Hybrid Surface Phonon and Plasmon Polariton Modes in Boron Nitride Nanotube and Graphene Monolayer Heterostructures

Yu Sun^{1,2,a)}, Zheng Zheng²⁾, Jiangtao Cheng³⁾, Jiansheng Liu²⁾

1 School of Information Science and Technology, Beijing Forestry University, Beijing 100083, China

2 School of Electronic and Information Engineering, Beihang University, Beijing 100191, China

3 Department of Mechanical and Energy Engineering, University of North Texas, Denton, Texas 76207, USA

The hybrid modes incorporating surface phonon polariton (SPhP) modes in boron nitride nanotubes (BNNTs) and surface plasmon polariton (SPP) modes in graphene monolayers are theoretically studied. The combination of the 1D BNNTs and 2D graphene monolayer further improves the modal characteristics with electrical tunability. Superior to the graphene monolayers, the proposed heterostructures supports single mode transmission with lateral optical confinement. The modal characteristics can be shifted from SPP-like toward SPhP-like. Both the figure of merit and field enhancement of hybrid modes are improved over 3 times than those of BNNT SPhP modes, which may further enable sub-wavelength mid-infrared applications.

Mid-infrared (IR) has great potentials in chemical and bio-molecular sensing, free space communication and thermal imaging for both civil and military purposes¹. However, most of these potential applications have been limited by the lack of mid-IR devices comparable to those in the near-IR regime². Surface polaritons are electromagnetic waves coupled to material charge oscillations, including the surface plasmon polaritons (SPPs) and surface phonon polaritons (SPhPs)³. Both SPPs and SPhPs exhibit high field enhancement and deep sub-wavelength confinement, which enables the next generation of mid-IR optical devices⁴.

The SPPs, collective oscillations of free electrons, are accessible in noble metals at visible and near-IR frequencies⁵. Recently, the SPPs have been extended to the mid-IR and THz spectral ranges by graphene⁶, a two dimensional (2D) layer of carbon atoms packed in hexagonal lattice⁷. The SPhPs originate from the phonon resonances at the mid-IR wavelengths in polar dielectric crystals, such as SiC, SiO₂ and hexagonal boron nitride (hBN)^{8,9}. The multiwall boron nitride nanotubes (BNNTs), a one-dimensional (1D) version of BN, supports SPhP modes with higher field confinement and enhancement than those at flat interfaces¹⁰. Both the effective index of 2D graphene SPP modes and 1D BNNT SPhP modes are capable of reaching ~70 in mid-IR frequencies^{5,6}.

Although the BNNTs provide a suitable nanoscale geometry to support single-mode transmission with lateral field confinement, the modal properties can only be statically controlled through the nanotube size or the supporting substrates¹¹.

^{a)} Email: sunyv@bjfu.edu.cn

The graphene monolayer can be dynamically tuned by the applied electric field⁵, but the 2D structure could not provide lateral field confinement. The graphene ribbon waveguide supports lateral optical confinement, yet only the extreme narrow ribbon can operate at single-mode region^{5,12}. It is challenging to fabricate, integrate and excite such a narrow ribbon.

To circumvent the above problems, we present the tunable hybrid modes in heterostructures incorporating 1D BNNTs and underlying 2D graphene monolayers. The hybrid modes originate from the plasmon-phonon coupling¹³. The hybrid modes exhibit high field confinement and enhancement. Superior to the graphene monolayers, the proposed heterostructures supports single mode transmission with lateral optical confinement. By tuning the chemical potential of graphene, the characteristics of hybrid modes can be shifted from SPP-like toward SPhP-like. By optimizing the chemical potential of the underlying graphene, the hybrid modes are capable of improving both the figure of merit and field enhancement over 3 times than those of BNNT SPhP modes. The hybrid modes may further enable mid-infrared applications far below the diffraction limit.

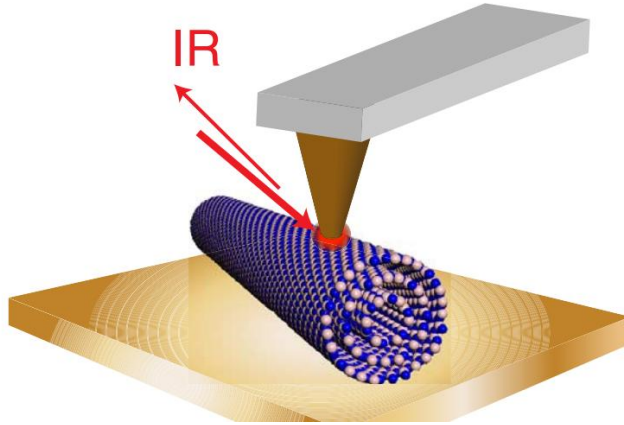


FIG. 1. Schematic of the proposed waveguide. (SCREENSHOT, TO BE UPDATE IN VER2)

The schematic of proposed heterostructures is shown in Fig. 1. The BNNT (25 nm diameter, 1/3 hollow)¹³ is separated from an underlying graphene monolayer by a 5nm air ($n=1$) gap¹⁴. An oscillator model is used to describe the dielectric function of hBN⁵. To focus on the unique tunability of graphene, the geometric parameters are fixed in this letter. The graphene is uniformly biased and tuned by the applied electric field using metallic gates shown in Fig. 1. The substrate is KCl ($n=1.466$)⁵, with air covering the rest regions. Graphene's complex conductivity is governed by the Kubo formula, which relates to the wavenumber ν , charged particle scattering rate Γ , temperature T , and chemical potential μ_c .¹⁵ The value of $\Gamma = \hbar q_e V_F / (2\mu E_F)$ is estimated from the measured impurity-limited DC graphene mobility $\mu \approx 10,000 \text{ cm}^2/(\text{Vs})$,¹⁶ where E_F is the Fermi levels, \hbar is the Planck's constant, q_e is the charge of an electron, V_F is the Fermi velocity ($\sim 10^8 \text{ cm/s}$ in graphene).¹⁷ The complex effective index n_{eff} -

ik_{eff} and field profiles of the hybrid modes are investigated at $\nu=1,420\text{cm}^{-1}$, $T=300\text{K}$ by the commercial finite-element method (FEM) solver COMSOLTM. Convergence tests are done to ensure that the boundaries and meshing do not interfere with the solutions.

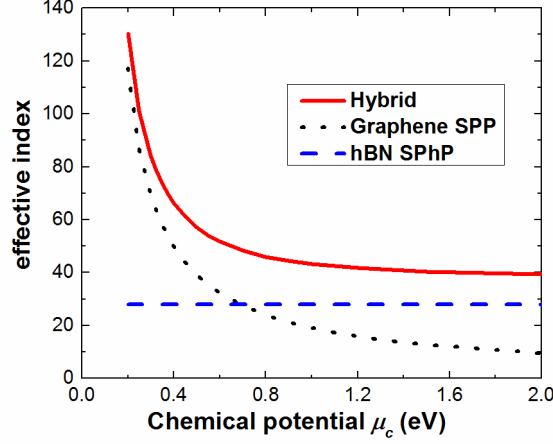


FIG. 2. Dependence of effective index on μ_c for the hybrid modes and un-hybrid SPP/SPhP modes.

The chemical potential of graphene μ_c can be tuned flexibly by external gates. The effective index n_{eff} of the hybrid mode with different μ_c are shown in Fig. 2. For illustration, the effective index of un-hybrid SPP modes supported by individual 2D graphene (without the BBNT in Fig. 1) and un-hybrid SPhP modes supported by individual 1D BBNT (without the graphene in Fig. 1) are also depicted. As shown in Fig. 2, the hybrid modes evolve from SPP-like to SPhP-like asymptotically with increasing μ_c . The BNNT operates in single mode condition, so only one SPhP mode can be excited and hybrids with graphene SPP mode. The single mode transmission is also confirmed by mode search using COMSOLTM.

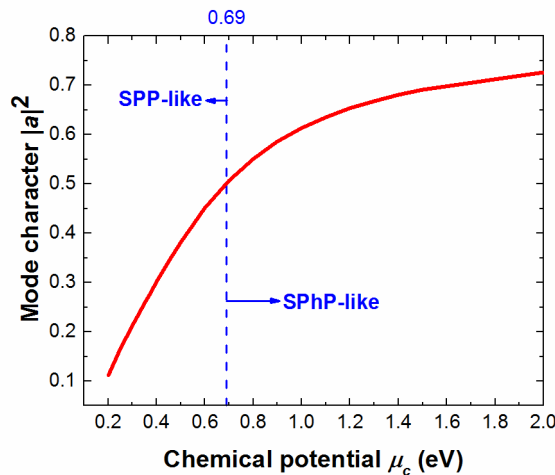


FIG. 3. Dependence of $|a|^2$ on μ_c for the hybrid mode as described by the coupled mode theory.

This hybridization can be modeled as the electromagnetically coupled oscillation between SPP and SPhP modes.⁹ The polarization originates from lattice displacement in the BNNT exerts a force on the free carriers of graphene via near field interaction,

and likewise the polarization originates from carrier displacement in the graphene exerts a force on the BNNT lattice. By tuning the chemical potential of graphene, the coupling can become constructive. Then the modal characteristics of the two constitutive polariton modes can be significantly enhanced and resulting the hybrid modes¹⁸. In order to gain a deeper understanding, the hybrid the modes are analyzed by coupled-mode theory¹⁹. The hybrid modes are modeled as a superposition of the graphene SPP modes and the BNNT SPhP modes: $n_{eff}(\mu_c)=an_{spp}(\mu_c)+bn_{sphp}$, where a and b are the amplitude of constituent SPP and SPhP modes respectively. The square norm of the SPP mode amplitude $|a|^2$ is a measure of hybridization:

$$|a|^2 = \frac{n_{eff}(\mu_c) - n_{spp}(\mu_c)}{[n_{eff}(\mu_c) - n_{spp}(\mu_c)] + [n_{eff}(\mu_c) - n_{sphp}]}. \quad (1)$$

In this respect, the modes are SPhP-like for $|a|^2 > 0.5$ and SPP-like otherwise. The dependence of $|a|^2$ on μ_c is shown in Fig. 3. The profile of $|a|^2$ confirms the transition between SPP-like and SPhP-like modes. The Figs. 4(a-d) depicts evolution of the electric field ($|E|$) profiles of hybrid modes with increasing μ_c . As shown in Fig. 4, the concentrations of $|E|$ field shift from the underlying graphene toward the upper BNNT with increasing μ_c . The $|E|$ profile of un-hybrid 1D BNNT SPhP modes are presented in Fig. 4(e) for comparison. The Fig. 3 also indicates the point of critical coupling: $\mu_c=0.69\text{eV}$. The $|E|$ field profiles of critical coupling are shown in Figs. 4(c). At the critical coupling point, the hybrid modes manifest equal SPP and SPhP characteristics ($|a|^2=|b|^2=0.5$), corresponding to $n_{spp}(\mu_c)=n_{sphp}=28.08$, indicating that two kinds of surface polaritons move in phase^{20,21}. The modes are highly confined and enhanced in the nanoscale air gap between the BNNT and graphene monolayer.

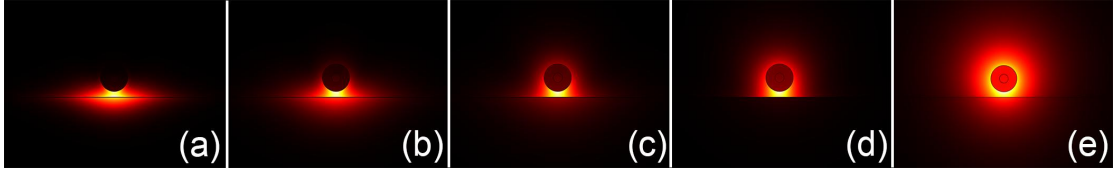


FIG. 4. $|E|$ profiles of hybrid modes with (a) $\mu_c=0.20\text{eV}$, (b) $\mu_c=0.35\text{eV}$, (c) $\mu_c=0.69\text{eV}$, (d) $\mu_c=2.00\text{eV}$; $|E|$ profile of un-hybrid 1D BNNT SPhP modes.

The figure of merit ($FoM=n_{eff}/2\pi k_{eff}$)²⁰ and field enhancement of the hybrid modes are shown in Fig. 5. The field enhancement is defined as the maximum of the electric field magnitude for a mode carrying $1\mu\text{W}$ power along the x axis shown in Fig. 1²⁰. By tuning the chemical potential of graphene, the figure of merit reaches the maximum value 2.37 when $\mu_c=0.35\text{eV}$. The corresponding field enhancement is up to $2.25 \times 10^7\text{V/m}$, which indicates that the field strength is dramatically enhanced as shown in Fig. 4(b). For comparison, the figure of merit and field enhancement of un-hybrid 1D BNNT SPhP mode is 0.69 and $7.18 \times 10^6\text{V/m}$, respectively. By the hybridization with the graphene SPP mode, both the figure of merit and field enhancement of BNNT SPhP mode are improved more than 3 times.

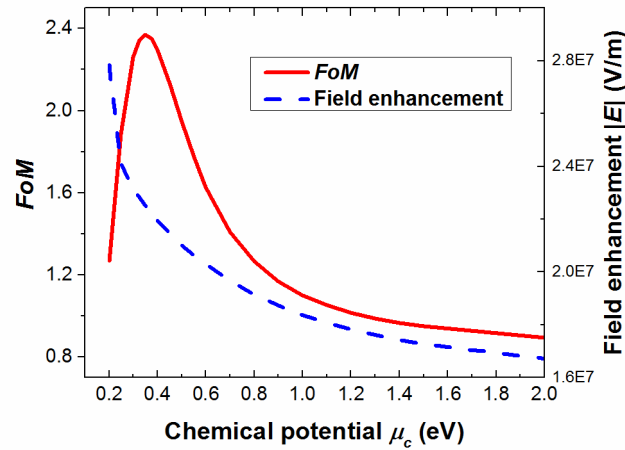


FIG. 5. Dependence of figure of merit (FoM) and field enhancement on μ_c .

In this letter, we report the tunable hybrid surface phonon and plasmon polariton modes supported by heterostructures incorporating BNNTs on a graphene monolayer. The combination of the 1D BNNTs and 2D graphene monolayer provides an avenue to further improve modal characteristics with electrical tunability. Superior to the graphene monolayers, the proposed heterostructures supports single mode transmission with lateral optical confinement. By optimizing the chemical potential of the underlying graphene, the hybrid modes is capable of improving both the figure of merit and field enhancement over 3 times than those of BNNT SPhP mode. The hybrid modes may further enable mid-infrared applications in guiding, concentrating and harvesting optical energy far below the diffraction limit.

This work was supported by the Fundamental Research Funds for the Central Universities (BLX2014-26/TD2014-01), 973 Program (2012CB315601) and NSFC (61435002/61107057/61221061/51378156).

- ¹ Majid Ebrahim-Zadeh and Irina T Sorokina, *Mid-infrared coherent sources and applications*. (Springer, 2008).
- ² A. Soref Richard, J. Emelett Stephen, and R. Buchwald Walter, *Journal of Optics A: Pure and Applied Optics* **8** (10), 840 (2006).
- ³ En-Kuang Tien, Yuewang Huang, Shiming Gao, Qi Song, Feng Qian, Salih K. Kalyoncu, and Ozdal Boyraz, *Opt. Express* **18** (21), 21981 (2010).
- ⁴ Sanja Zlatanovic, Jung S Park, Slaven Moro, Jose M Chavez Boggio, Ivan B Divliansky, Nikola Alic, Shayan Mookherjea, and Stojan Radic, *Nature Photonics* **4** (8), 561 (2010).
- ⁵ Xiaoji G. Xu, Behnood G. Ghamsari, Jian-Hua Jiang, Leonid Gilburd, Gregory O. Andreev, Chunyi Zhi, Yoshio Bando, Dmitri Golberg, Pierre Berini, and Gilbert C. Walker, *Nat Commun* **5** (2014).
- ⁶ D. Caldwell Joshua, Lindsay Lucas, Giannini Vincenzo, Vurgaftman Igor, L. Reinecke Thomas, A. Maier Stefan, and J. Glembocki Orest, *Nanophotonics* **0** (0) (2014).
- ⁷ W. L. Barnes, A. Dereux, and T. W. Ebbesen, *Nature* **424** (6950), 824 (2003).
- ⁸ A. N. Grigorenko, M. Polini, and K. S. Novoselov, *Nat Photon* **6** (11), 749 (2012).

- 9 K. S. Novoselov, A. K. Geim, S. V. Morozov, D. Jiang, Y. Zhang, S. V. Dubonos, I. V. Grigorieva, and A. A. Firsov, *Science* **306** (5696), 666 (2004).
- 10 S. Dai, Z. Fei, Q. Ma, A. S. Rodin, M. Wagner, A. S. McLeod, M. K. Liu, W. Gannett, W. Regan, K. Watanabe, T. Taniguchi, M. Thiemens, G. Dominguez, A. H. Castro Neto, A. Zettl, F. Keilmann, P. Jarillo-Herrero, M. M. Fogler, and D. N. Basov, *Science* **343** (6175), 1125 (2014).
- 11 Paloma A. Huidobro, Maxim L. Nesterov, Luis Martín-Moreno, and Francisco J. García-Vidal, *Nano Letters* **10** (6), 1985 (2010).
- 12 Ashkan Vakil and Nader Engheta, *Science* **332** (6035), 1291 (2011).
- 13 A. Yu Nikitin, F. Guinea, F. J. García-Vidal, and L. Martín-Moreno, *Physical Review B* **84** (16), 161407 (2011).
- 14 Victor W. Brar, Min Seok Jang, Michelle Sherrott, Josue J. Lopez, and Harry A. Atwater, *Nano Letters* **13** (6), 2541 (2013).
- 15 R. Geick, C. H. Perry, and G. Rupprecht, *Phys. Rev.* **146**, 543 (1966).
- 16 H. H. Li, *Journal of Physical and Chemical Reference Data* **5** (2), 329 (1976).
- 17 L. A. Falkovsky and A. A. Varlamov, *Eur. Phys. J. B* **56** (4), 281 (2007).
- 18 JS Gómez-Díaz, M Esquiús-Morote, and J Perruisseau-Carrier, *Opt. Express* **21** (21), 24856 (2013).
- 19 Victor W. Brar, Min Seok Jang, Michelle Sherrott, Seyoon Kim, Josue J. Lopez, Laura B. Kim, Mansoo Choi, and Harry Atwater, *Nano Letters* **14** (7), 3876 (2014); Yusheng Bian, Zheng Zheng, Ya Liu, Jiansheng Liu, Jinsong Zhu, and Tao Zhou, *Opt. Express* **19** (23), 22417 (2011).
- 20 Rupert F Oulton, Volker J Sorger, DA Genov, DFP Pile, and X Zhang, *Nature Photonics* **2** (8), 496 (2008).
- 21 Yu Sun, Zheng Zheng, Jiangtao Cheng, Jianwei Liu, Jiansheng Liu, and Shuna Li, *Applied Physics Letters* **103** (24), 241116 (2013).